CHAPTER-VII

Magnetic Behaviour and Magnetic Structure

7.1 Introduction

As discussed in Chapter I, the presence of spatially modulated spiral spin structure cancels out the net macroscopic magnetization due to the G-type canted antiferromagnetic structure of $BiFeO_3$. Because of this there is no linear magnetoelectric coupling [Popov et al. (1993)]. One of the possible ways to release the latent magnetization locked-in the modulated spiral spin structure of $BiFeO_3$ is by chemical substitution or forming solid solutions with, say, another ABO_3-type perovskite [Sosnowska et al. (2002)]. Solid solutions of $BiFeO_3$ with $Pb(Fe_{0.5}Nb_{0.5})O_3$ show order of magnitude lower values of remanent magnetization [Smolenskii et al. (1965), Paik et al. (2009)] in comparison to other solid solutions such as (1-x)$BiFeO_3$-x$BaTiO_3$(BF-xBT) [Singh et al. (2014)], $(Bi_{1-x}Ca_x)(Fe_{1-x}Ti_x)O_3$ [Wang et al. (2012)], $(Bi_{0.25}La_{0.25}Pb_{0.5})(Fe_{0.5}Ti_{0.5})O_3$ [Wang et al. (2012)] and $(Bi_{0.8}La_{0.2})$(Fe,Ga)-45%$PbTiO_3$ [Wang et al. (2005)]. Weak ferromagnetism in solid solutions of $BiFeO_3$ is of great interest since it can lead to linear magnetoelectric coupling. There is no systematic study of the magnetic behavior of BF-xPFN solid solutions using M (T) and M-H measurements. The magnetic structures of $BiFeO_3$ and its derived systems (e.g. $(Bi_{1-x}Pb_x)(Fe_{1-x}Ti_x)O_3$, $Bi_{0.93}La_{0.07}FeO_3$, $Bi_xCa_{1-x}FeO_3$, $BiFe_{1-x}Mn_xO_3$, BF-xBT etc.) have been investigated by several workers [Sosnowaska et al. (1996); Sosnowaska et al. (2002); Comyn et al. (2008); Chen et al. (2009); Bhattacharjee et al. (2010); Singh et al. (2014)], but the magnetic structures of the different phases of BF-xPFN solid solutions have not been studied using neutron diffraction. The present chapter

presents the results of a comprehensive study of the magnetic behavior of BF-xPFN solid solutions over the entire composition range.

7.2 Experimental

The DC magnetization (M) measurements were carried out as a function of temperature using a vibrating sample magnetometer (VSM-7410, Lakeshore) at a heating rate of 2 K/minute. The M (T) measurement was performed by applying H = 2 kOe magnetic field. The field dependence of magnetization (M-H) of BF-xPFN samples at room temperature were measured in the range ± 20 kOe.

High-resolution neutron powder diffraction (NPD) data were collected on BF-xPFN solid solution for x = 0.20 and 0.90 compositions using SPODI powder diffractometer at FRM-II, Germany [Hoelzel et al. (2007)]. For x = 0.20, high-resolution NPD data were collected in the temperature range 300-1173 K while for x = 0.90, high resolution NPD data were collected only at room temperature. The incident neutron wavelength was 1.5482 Å as obtained from Ge 551 reflection of vertically focused monochromator at 155° take-off. Cylindrical sample holder (Niobium (Nb) with 50μm wall thickness, 40mm height, and 10 mm diameter) contained approximately 20g of the sample during the experiment. The data were collected at a step of 0.05° in the 2θ range from 5 to 130°.

High flux neutron powder diffraction (NPD) patterns were collected for BF-0.5PFN over the temperature range 275-655 K using the Wombat diffractometer (λ = 1.78 Å) at the OPAL reactor (ANSTO, Australia). However, for BF-0.8PFN neutron powder diffraction data was collected in the temperature range 2-300 K by

using same diffractometer at the incident wavelength λ = 2.41 Å. For the high flux data collection on WOMBAT, 3 to 5 g of sample was used in a cylindrical Vanadium can. Here, the data were collected at a step of 0.125° in the 2θ range from 15 to 125°.

7.3 Rietveld refinement of neutron powder diffraction data: Magnetic structure refinement

Neutron powder diffraction data were analyzed by Rietveld refinement technique using FULLPROF software package [Carvajal (2010)]. For the neutron diffraction data "Thompson-Cox-Hastings pseudo-Voigt with Axial divergence asymmetry" function was used for peak profile while the linear interpolation method was used to account the background. The magnetic structure of a given neutron diffraction data in the magnetic phase (for $T < T_N$) was determined by following steps:

(i) Refinement of the crystal structure using neutron diffraction data (NPD) of a sample collected in the paramagnetic phase ($T > T_N$) or x-ray diffraction data of the magnetic phase of the sample to get all the relevant structural and profile parameters.

(ii) The propagation vector (k) is determined using the peak positions of the additional magnetic peaks by program K-search or by trial and error method with an additional phase in the PCR file treated in the Le-Bail fit (LBF) mode to account for all the magnetic reflections with respect to the nuclear unit cell.

(iii) Basis vectors of the irreducible representations (irreps) of the propagation vector group (G_k) are determined by using program BASEIREPs or SARAh representational analysis program [Wills (2000)].

(iv) The magnetic structure was refined using the symmetry information obtained in step (III) using trial and error methods. The PCR file is modified by selecting the basis vectors of a particular irreducible representation or by mixing the basis vectors of the irreducible representations by using the SARAh representational analysis program.

(v) Refinement of the coefficients of the basis functions by fixing all the structural and profile parameters and checking if the calculated magnetic peaks have intensities close to the observed ones. If not, the magnetic model was revisited.

7.4 Results and discussion

7.4.1 Magnetic behavior of BF-xPFN at room temperature

$BiFeO_3$ shows linear M-H response because of the presence of the spatially incommensurate modulated spiral spins structure of an approximate wavelength ~ 620 Å [Lebeugle et al. (2007)]. Fig. 7.1 depicts the room temperature M-H response of the BF-xPFN solid solutions for $0.10 \leq x \leq 0.96$ with applied magnetic field (H) in the range ± 5 kOe. The opening of the M-H loop is observed in all the compositions in the range $0.10 \leq x \leq 0.96$. However, unlike the ferromagnetic materials, the hysteresis loop of BF-xPFN at room temperature does not show saturation of magnetization.

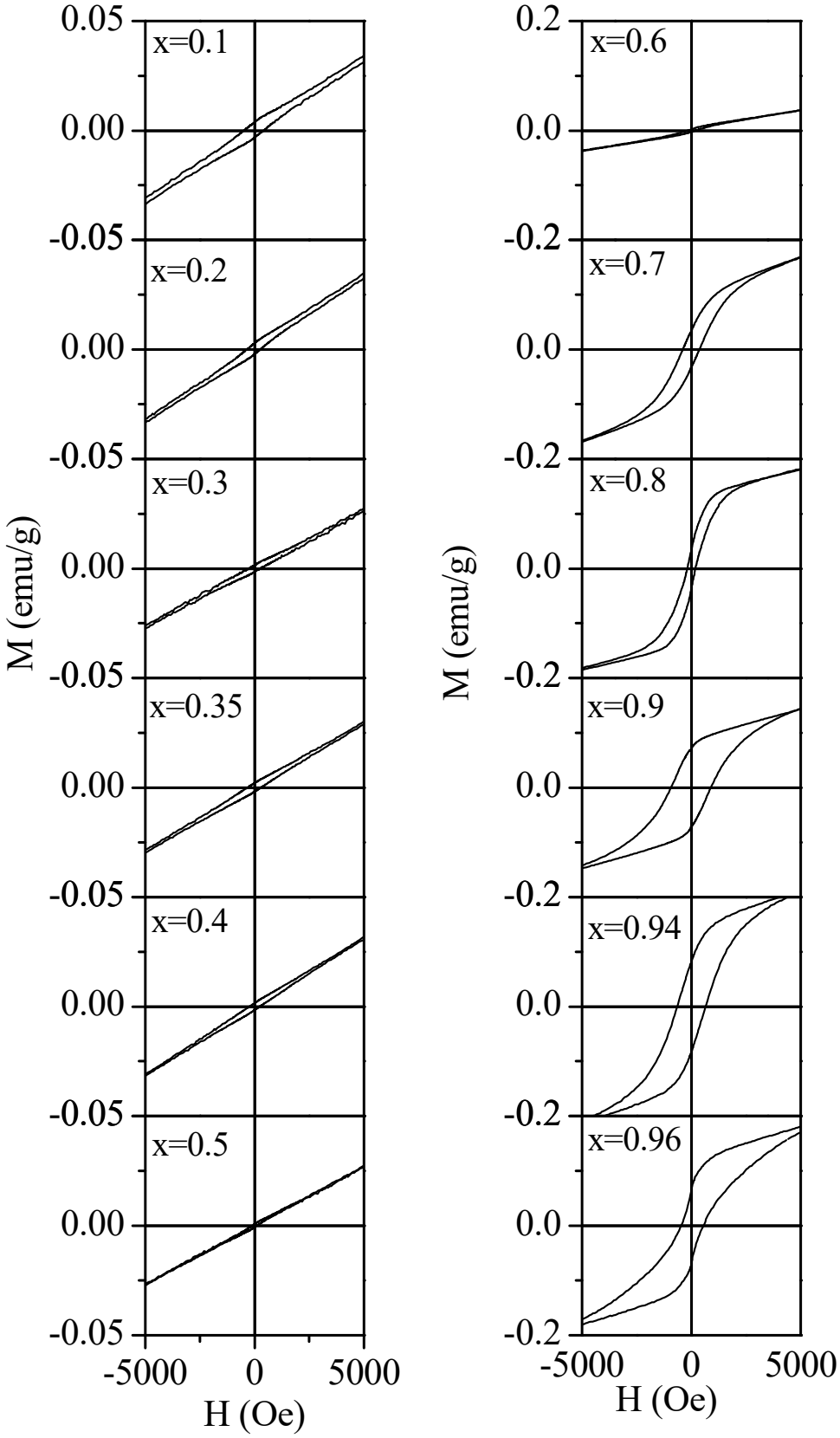

Fig. 7.1 Magnetic hysteresis (*M-H*) loops of BF-xPFN solid solutions at room temperature.

Instead, the magnetization varies linearly as a function of applied field at high fields as can be seen from the Fig. 7.1. This is a characteristic of weak ferromagnetism in canted antiferromagnetic systems [Serrao et al. (2005)]. The remanent magnetization (M_r) initially increases with increasing x from zero value for $BiFeO_3$ to the maximum value (~ 0.0038 emu/g) for x = 0.10 after which it decreases with increasing x and achieves a minimum for x ≈ 0.50 as depicted in Fig. 7.2. On increasing the PFN content (x) further, the M_r starts increasing and shows another peak at x ~ 0.90 after which it starts decreasing. The value of M_r at the first peak at x = 0.10 is an order of magnitude smaller than that at the second peak.

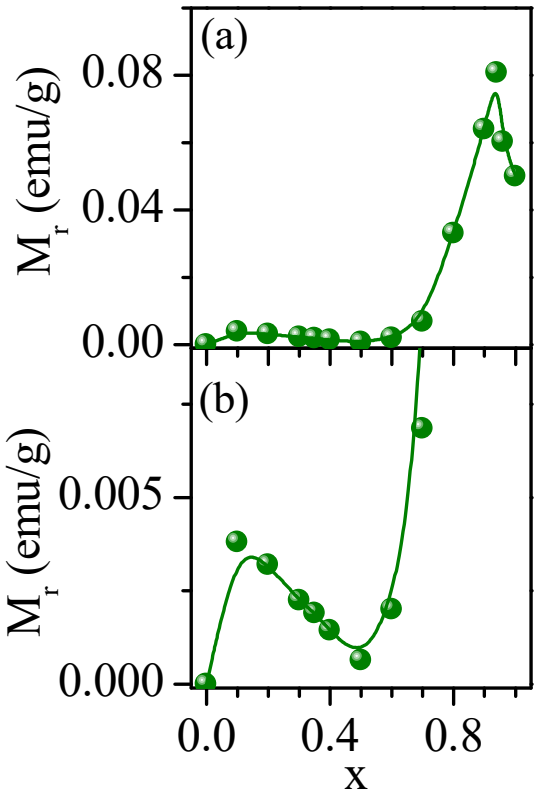

Fig. 7.2 Variation of (a) remanent magnetization (M_r) with composition. (b) The M_r vs x plot on a zoomed scale.

The observation of weak ferromagnetic behavior in BF-xPFN solid solutions is due to partial or complete melting of the spiral spin structure of $BiFeO_3$ on $Pb(Fe_{0.5}Nb_{0.5})O_3$ substitution. In single crystals of $BiFeO_3$, application of a high magnetic field ($H \geq 20$ Tesla) along [001] has been shown to induce a phase transition from the spatially modulated antiferromagnetic spiral spin structure to a spatially homogeneous antiferromagnetic structure [Popov et al. (1993)]. This transition results in the release of the locked-in magnetization, which is reported to be of the order of 0.3 emu/g at 10 K [Wang et al. (2005)]. Yet another way to destroy the spiral spin structure of $BiFeO_3$ is to use nanocrystalline $BiFeO_3$ having particle sizes smaller than the wavelength (~ 62 nm) of the spiral-modulated spin structure. The $BiFeO_3$ nanoparticles with size less than 62 nm have been reported to exhibit large values of spontaneous magnetization (M_S ~ 1.55 emu/g at 300 K) in comparison with the particles having sizes greater than 62 nm [Park et al. (2007)] because of enhanced contribution from the surface layers as well. The spiral spin structure seems to be suppressed under epitaxial constraints which are also reported to lead to saturation magnetization values of M_S ~ 0.06 μ_B/Fe [Eerenstein et al. (2005)]. Yet another convenient way of destroying the spiral spin structure is by chemical substitutions leading to weak ferromagnetism and linear magnetoelectric coupling. Doping of $BiFeO_3$ with La^{3+} is known to produce weak ferromagnetism in $Bi_{0.7}La_{0.3}FeO_3$ [Sosnowska et al. (1993)]. In the mixed system $(Bi_{0.8}La_{0.2})(Fe,Ga)O_3$-45% $PbTiO_3$, a remanent magnetization (M_r) of ~ 0.15 and 0.3 emu/g at T = 300 K and 5 K, respectively, have also been reported [Wang et al. (2005)]. The fact that the values of M_r (~ 0.3 emu/g) reported at low

temperatures in $BiFeO_3$ solid solutions are comparable to that in pure $BiFeO_3$ at 10 K after the destruction of spiral spin structure under intense magnetic field of ~ 20 T suggests that transition from the modulated spiral spin structure to homogenous spin structure occurs by chemical substitutions also. It also suggests that M_r values close to 0.15 emu/g reported at room temperature in $BiFeO_3$ solid solutions are due to the destruction of the spiral spin structure. This has been confirmed by neutron scattering studies in $Bi(Mn_{0.1}Fe_{0.9})O_3$ and $(Bi_{0.8}Ba_{0.2})$ $(Fe_{0.8}Ti_{0.2})O_3$ [Sosnowska et al. (2002), Singh et al. (2011)]. Similarly in the $(Bi_{1-x}Ba_x)$ $(Fe_{1-x}Ti_x)O_3$ (BF-xBT) mixed system, remanent magnetization has been reported for x = 0.10 [Singh et al. (2008)] and higher x values with a maximum value of ~ 0.15 emu/g for x = 0.20 [Wang et al. (2005)]. More recently, in 20% $CaTiO_3$ substituted $BiFeO_3$, remanent magnetization M_r ~ 0.18 emu/g and ~ 0.26 emu/g have been reported at 300 K and 5 K, respectively [Wang et al. (2012)].

However, the values of M_r in BF-xPFN solid solutions in the composition range $0.10 \leq x \leq 0.60$ at room temperature is approximately two orders of magnitude less than that reported due to the melting of the spiral spin structure of $BiFeO_3$ either by doping or by application of intense magnetic field ($H \geq 18$ T) [Popov et al. (1993), Wang et al. (2005)]. The observation of very low value of M_r in the BF-xPFN solid solutions suggests that either the canting angle is very small or spiral spin structure of $BiFeO_3$ is only partially suppressed even after 60% substitution with PFN. The observation of small remanent magnetisation in BF-xPFN solid solution however suggests that the $Pb(Fe_{0.5}Nb_{0.5})O_3$ substitution also

transforms the modulated spin structure of $BiFeO_3$ to partially or completely homogenous spin structure for x close to 0.10.

7.4.2 Room temperature magnetic structure of BF-xPFN

Fig. 7.3 depicts the neutron powder diffraction patterns of BF-xPFN for x = 0.2, 0.5, 0.8 and 0.9 collected at room temperature. Since the data were collected at different wavelengths, they are plotted against inverse of d-spacings on the horizontal axis in the range 0.2 to 0.60$Å^{-1}$. It can be seen from the figure that for x= 0.2 an additional peak (marked with an asterisk '*') other than the main perovskite peaks, is present around 1/d = 0.215 $Å^{-1}$. This is the strongest magnetic diffraction peak coming from the antiferromagnetic ordering. The intensity of this magnetic peak decreases with increasing concentration of $Pb(Fe_{0.5}Nb_{0.5})O_3$ (i.e., x) and vanishes for x = 0.90. This suggests that the strength of antiferromagnetic ordering in BF-xPFN decreases with increasing $Pb(Fe_{0.5}Nb_{0.5})O_3$ content. For compositions with x = 0.90, the antiferromagnetic ordering completely vanishes. The observations of the neutron diffraction data indicates that antiferromagnetic ordering at room temperature persists up to $0.80 \leq x < 0.90$. This implies that the non-zero M_r up to x = 0.80 shown in Fig. 7.2 (a) and Fig. 7.2 (b) is due to spin canting. However, the spin canting angle is usually very small in $BiFeO_3$ solid solutions [Lee et al. (2010)] and cannot be determined from Rietveld analysis. The fact that M_r and the H_C increases abruptly at $x \approx 0.90$ in Fig. 7.1 and Fig. 7.2 also suggests that the nature of magnetic ordering changes for x > 0.80.

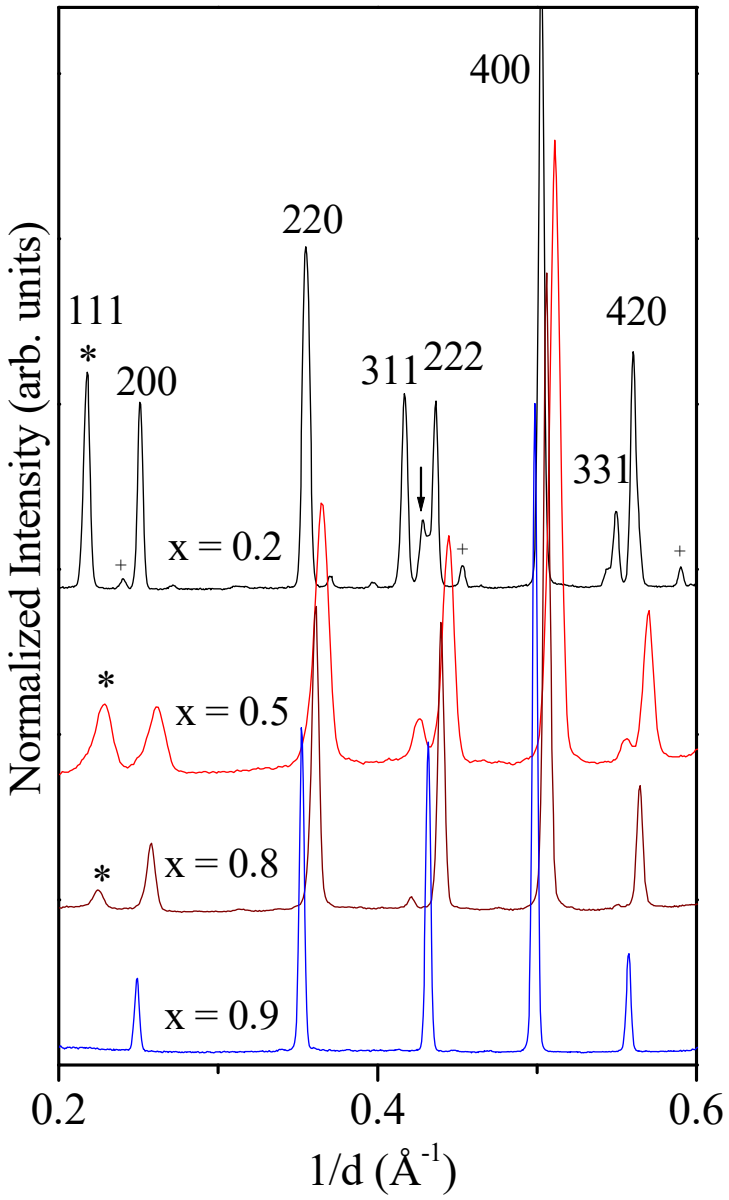

Fig. 7.3 Neutron powder diffraction patterns of BF-xPFN for x = 0.20, 0.50, 0.80 and 0.90 collected at room temperature. Arrow indicates the Nb sample holder peak while the symbol (+) indicate the small trace of Fe_2O_3 impurities. The asterisk (*) marked peak is the strongest magnetic peak. All the indices are with respect to a doubled pseudocubic cell.

7.4.3 Magnetic structure of the rhombohedral phase ($0.10 \leq x \leq 0.32$)

For determining the magnetic structure of BF-xPFN in the rhombohedral phase with R3c space group, we consider x = 0.20 composition as the representative composition. The room temperature neutron powder diffraction pattern of BF-0.2PFN was analyzed by Rietveld technique using FULLPROF package [Carvajal (2010)]. We have used hexagonal setting for the R3c space group with lattice parameters $a_H \sim \sqrt{2}\, a_p$, $b_H \sim \sqrt{2}\, a_p$ and $c_H \sim 2\sqrt{3}\, a_p$, where a_p is the pseudocubic cell parameter. The positional coordinates of the atoms in the asymmetric unit are: Bi/Pb: (0, 0, 0.25+s), Fe/Nb: (0, 0, t) and O: (0.16666-2e-2d, 0.3333-4d, 0.0833). The polar displacements of the cations are described by the parameters 's' and 't' whereas 'd' and 'e' represent the octahedral distortion and the octahedral tilt angle $\Phi = \tan^{-1}(4\sqrt{3}e)$ along $[111]_{pc}$ axis, respectively [Megaw et al. (1975)]. The initial lattice parameters and atomic coordinates were based on Rietveld refinements of synchrotron and laboratory x-ray diffraction data at room temperature. The magnetic reflections were indexed in terms of an additional phase considered during the nuclear structure refinements. The magnetic Bragg peaks were indexed with k = (0,0,0) propagation vector having identical unit cell and the structural parameters as the R3c nuclear unit cell. The magnetic structures compatible with the R3c symmetry are determined by the representational analysis technique. For the propagation vector k = (0,0,0), the little group G_k formed by those element of the space group G_0 (R3c) that leave 'k' invariant or only changed by a translation of the reciprocal lattice coincide with the space group R3c.

For k = (0,0,0), the irreducible representations of the little group G_k are given in Table 7.1.

Table 7.1 Irreducible representation of the little group G_k. The propagation vector is k = (0,0,0). Phase factor: a = exp(2πi/3); b = exp(4πi/3)

Ireps	Symmetry element of G_k					
	1	3+0,0,z	3-0,0,z	c x,-x,z	c x,2x,z	c x,x,2z
Γ_1	1	1	1	1	1	1
Γ_2	1	1	1	-1	-1	-1
Γ_3	1 0 0 1	a 0 0 b	b 0 0 a	0 1 1 0	0 b a 0	0 a b 0

In the R3c space group with hexagonal unit cell, the magnetic ion Fe^{3+} occupies the 6a Wyckoff site with general positions (0,0,z), and (0,0,z+1/2). The magnetic reducible representation Γ_{mag} for the 6a Wyckoff site for k = (0,0,0) can be decomposed as direct sum of three irreducible representations

$$\Gamma_{mag}(6a/Fe)=1\Gamma_1^1+1\Gamma_2^1+2\Gamma_3^2 \qquad (7.1)$$

The basis vectors associated with each irreducible representation, obtained by following the projection operator technique implemented in the SARAh [Wills,(2000)], are given in Table 7.2. The Γ_1 and Γ_2 representations are one dimensional whereas Γ_3 representation is two dimensional. Γ_1 and Γ_2 correspond to single basis vector magnetic structures while Γ_3 corresponds to four basis vector magnetic structure [Bertaut (1962), Bertaut (1968)].

Table 7.2 Basis vectors of the irreducible representations of the space group R3c appearing in the magnetic representation at the Wyckoff position 6a for the wave vector k = (0, 0, 0).

Ireps	Basis vector	Atom 1 (0, 0, z)			Atom 2 (0, 0, z+1/2)		
		m_x	m_y	m_z	m_x	m_y	m_z
Γ_1	ψ_1	0	0	3	0	0	-3
Γ_2	ψ_2	0	0	3	0	0	3
Γ_3	ψ_3	$\frac{3}{2}-i\frac{\sqrt{3}}{2}$	$-i\sqrt{3}$	0	0	0	0
	ψ_4	0	0	0	$-\frac{3}{2}-i\frac{\sqrt{3}}{2}$	$-\frac{3}{2}+i\frac{\sqrt{3}}{2}$	0
	ψ_5	0	0	0	$-\frac{3}{2}+i\frac{\sqrt{3}}{2}$	$-\frac{3}{2}-i\frac{\sqrt{3}}{2}$	0
	ψ_6	$\frac{3}{2}+i\frac{\sqrt{3}}{2}$	$+i\sqrt{3}$	0	0	0	0

The basis vectors of the irreducible representation Γ_3 are related in the pairs as $\Psi_3^* = \Psi_6$ and $\Psi_4^* = \Psi_5$ and therefore simplify the refinement of the mixing coefficients. The observed magnetic peaks in the neutron powder diffraction pattern shown in Fig. 7.3 cannot be explained in terms of the irreducible representations Γ_2, since it represents a ferromagnetic ordering. This leaves Γ_1 and Γ_3 as the likely representations for BF-0.2PFN. Both the representations correspond to G-type antiferromagnetic ordering. However, for Γ_1 the spins are parallel to $(001)_{hex}$ (or $[111]_{pc}$) direction while the spins are in the $(001)_{hex}$ ($(111)_{pc}$) plane for Γ_3 (see Fig. 7.4).

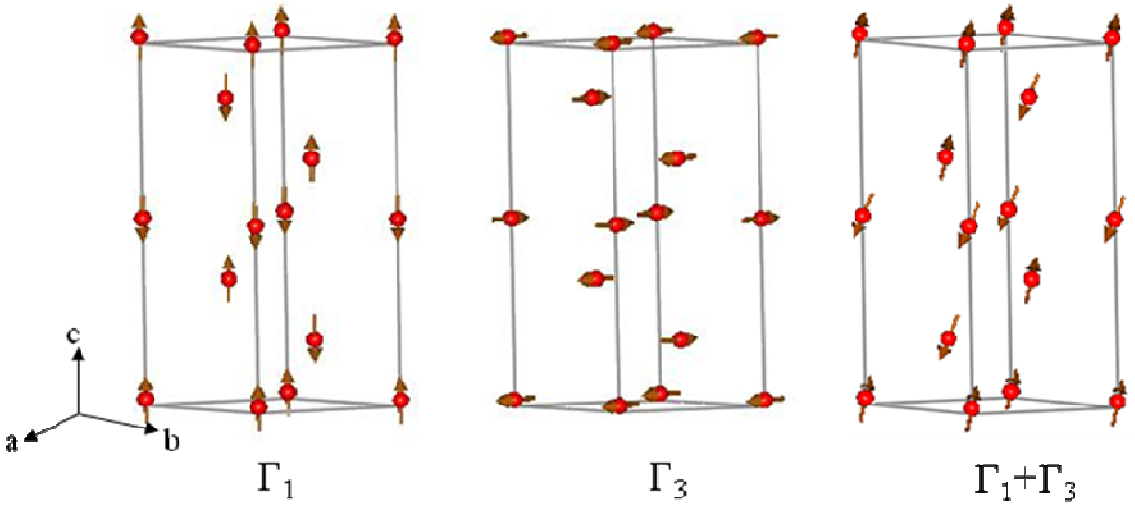

(a) (b) (c)

Fig. 7.4 Magnetic structures of BF-0.2PFN corresponding to (a) representation Γ_1 for the model I with magnetic moments parallel to $[001]_h$, (b) representation Γ_3 for model III with the magnetic moments in $(001)_h$ plane and (c) representation $\Gamma_1 + \Gamma_3$ for model IV with magnetic moments having two components, one of them is parallel to $[001]_h$ direction and another components lies in $(001)_h$ plane.

Fig. 7.5(a-d) depicts the fits between the observed and calculated profiles obtained by Rietveld refinement for Γ_1, Γ_2, Γ_3 and mixed $\Gamma_1 + \Gamma_3$ representations. The neutron diffraction data contains reflections of the sample holder made of Nb and small traces of Fe_2O_3. The peak positions of these two phases do not overlap with peak positions of nuclear and magnetic peaks of BF-0.2PFN. The Nb and Fe_2O_3 were considered as additional phases with space groups $I\,m\bar{3}\,m$ and $R\,\bar{3}\,c$, respectively. As expected, the magnetic structure corresponding to the representation Γ_2 failed to model the magnetic reflections as can be seen from Fig.

7.5 (b). The fit between the observed and calculated profiles are quite good corresponding to the representations Γ_1 and Γ_3 (see Fig. 7.5 (a) and Fig. 7.5 (c)). The values of the R-factors for the refinement corresponding to the representation Γ_1 (model I) are: R_{wp} = 7.3, χ^2 = 2.53 and $R_{magnetic}$ = 2.48. The value of ordered magnetic moment per Fe atom located at (0,0,Z) and (0,0,Z+1/2) are 3.72(3) μ_B and -3.72(3) μ_B, respectively. The values of the R-factors corresponding to the irreducible representation Γ_3 (model III) are: R_{wp} = 7.10, χ^2 = 2.45 and $R_{magnetic}$ = 2.7 which are comparable to the magnetic structure of the irreducible representation Γ_1 (model I). The structural parameters and coordinates obtained after Rietveld refinement are nearly the same (within standard deviations) as obtained for model I. Also, the ordered magnetic moment for model III is 3.8(1) μ_B, which is close to that for model I (~ 3.72(3) μ_B).

As discussed earlier, the magnetic measurements on BF-0.2PFN show a weak ferromagnetic loop suggesting canting of spins and suppression of the spiral spin structure. The canting of antiferromagnetic spins is permitted by the R3c symmetry only if the sublattice magnetizations are oriented in the $(001)_h$ planes, i.e. model III [Dzyaloshinskii (1957), Ederer and Spaldin (2005)]. Therefore, out of the two models (Γ_1 and Γ_3) described above, the presence of weak ferromagnetism in BF-0.2PFN can only be explained by the magnetic structure corresponding to irreducible representation Γ_3 in which the sublattice magnetizations are oriented in the $(001)_h$ planes.

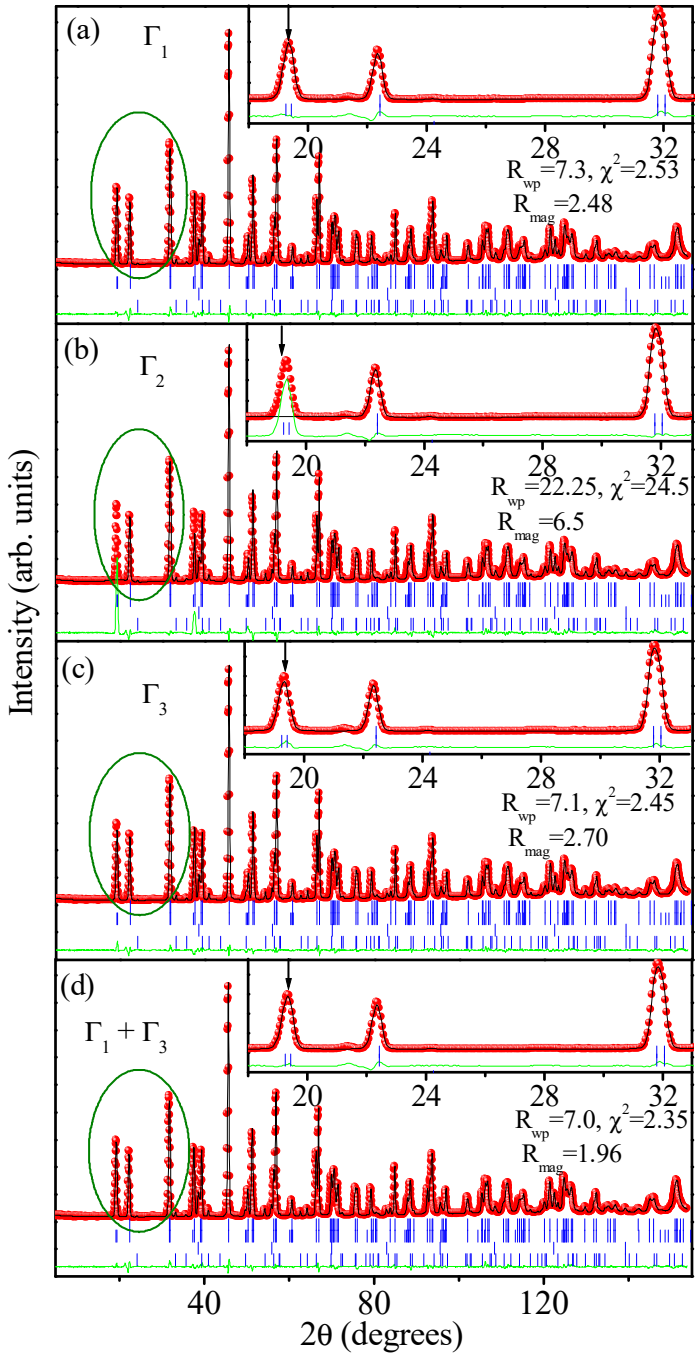

Fig. 7.5 Observed (dots), calculated (solid line) and difference (bottom line) profiles obtained from the Rietveld refinement using neutron powder diffraction data at room temperature corresponding to the irreducible representation (a) Γ_1 (model I), (b) Γ_2 (model II), (c) Γ_3 (model III) and (d) $\Gamma_1 + \Gamma_3$ (model IV). The vertical tick marks above the difference profile correspond to the positions of Bragg reflections for nuclear (top) and magnetic (second top) structures and below it tick marks indicate the peaks positions of Nb sample holder and iron oxide impurity (lowest tick marks). Insets depict the zoomed portion of the fitted profiles enclosed by ellipses. The statistical parameters are also given for Γ_1, Γ_2, Γ_3 and $\Gamma_1 + \Gamma_3$ with their respective profile fits.

Alternatively, the true magnetic structure may correspond to an exchange multiplet in which both the irreducible representations (Γ_1 and Γ_3) contribute. Such models, though not possible within the framework of single irreducible representations based definition of order parameter in Landau theory, are not uncommon. For example, the R3c phase of BF-0.2PFN results from simultaneous freezing of zone center polar mode Γ_{4-} and the zone boundary antiferrodistortive mode R_{4+} none of which can be said to be secondary to the other i.e., it is not possible to call one of the representations as the primary order parameter [Patel et al. (2010)]. The consideration of such a model for the magnetic structure of BF-xPFN allows deviation of the magnetic moment from the hexagonal axis and permits canting and weak ferromagnetism. Accordingly, we carried out Rietveld refinement of the nuclear and magnetic structures using mixture of Γ_1 and Γ_3 representations also. The fit is shown in Fig. 7.5(d) which is slightly better than that for Γ_1 or Γ_3 with R_{wp} = 7.0%, χ^2 = 2.35 and R_{mag} = 1.96. The ordered magnetic moment (μ_B = 3.74(3)) and the positional coordinates are, however, similar to the single irreducible representation models. The magnetic structure is schematically shown in Fig. 7.4 (c). The results of the Rietveld analysis of neutron diffraction data of BF-xPFN for x = 0.20 are given in Table 7.3.

Table 7.3 Refined structural parameters for x = 0.20, 0.50, 0.80 and 0.90 compositions of BF-xPFN.

x	0.20	0.50	0.80	0.90
Space Group	R3c a=b≠c, α=β=90°, γ=120°	$Pm\bar{3}m$ a=b=c, α=β=γ=90°		
a (Å)	5.60836(2)	3.9858(1)	4.0090(7)	4.01057(2)
b (Å)	13.89578(8)	-	-	-
Bi/Pb (x)	0.0000	0.0220(1)	0.0410(1)	0.0379(1)
Bi/Pb (y)	0.0000	0.0220(1)	0.0410(1)	0.0379(1)
Bi/Pb (z)	0.2918(1)	0.0841(2)	0.0410(1)	0.0379(1)
Fe/Nb (z)	0.01672(8)	0.50	0.50	0.50
O (x)	0.2253(2)	0.5431(5)	0.5271(2)	0.50
O (y)	0.3493(2)	0.5431(5)	0.5271(2)	0.50
O (z)	0.083333	0.0000	0.0000	0.0000
B (Bi/Pb)	2.29(2)	2.27(4)	2.55(6)	1.95(3)
B (Fe/Nb)	0.57(3)	0.96(3)	0.88(5)	0.41(1)
B (O)	1.23(5)	3.22(5)	2.90(4)	1.29(2)
Fe-O_1	1.9529(2)	2.0137(2)	2.0093(2)	2.0049(2)
Fe-O_2	2.1059(2)	2.0137(2)	2.0093(3)	2.0049(2)
Fe-O-Fe	158.96	162.97	174.02	180.0
μ_{Fe} (μ_B)	3.74(3)	3.0(2)	1.5(4)	-
R_{wp} (%)	7.000	6.00	5.7	6.000
χ^2	2.35	9.18	1.66	1.70
R_{mag} (%)	1.96	3.30	3.4	-

7.4.4 Magnetic structure of the cubic like phase for $0.40 \leq x < 0.80$)

The x = 0.50 composition was used as a representative composition for the magnetic structure in the composition range $0.40 \leq x < 0.80$. Since, it has been shown that the room temperature crystal structure of BF-0.5PFN is cubic ($Pm\bar{3}m$ space group) with A-site and O-site local disorders, we used cubic phase with $Pm\bar{3}m$ space group for the nuclear structure refinement. We have used isotropic thermal parameters for refining the nuclear structure. The additional peaks (the magnetic Bragg peaks) were indexed with a propagation vector k = (0.5,0.5,0.5) referred to the space group $Pm\bar{3}m$. The propagation vector k = (0.5,0.5,0.5) means the magnetic unit cell is two times larger in a, b and c directions, respectively, than the nuclear unit cell. The magnetic structure compatible with $Pm\bar{3}m$ symmetry are determined by representation analysis technique discussed by Singh et al. (2013). In the $Pm\bar{3}m$ space group, the magnetic ions Fe^{3+} occupy the 1b Wyckoff site with general positions (0.5,0.5,0.5). The decomposition of the magnetic representation Γ_{mag} in terms of irreducible representations Γ_k for the 1b site of the cubic symmetry is as follows [Singh et al. (2013)]:

$$\Gamma_{mag}\,(1b/\,Fe) = 1\,\Gamma_{7}^{3} \qquad (7.2)$$

For the k = (0.5,0.5,0.5) propagation vector, there is only one possible magnetic structure corresponding to the irreducible representation Γ_7 . The different basis vectors associated with irreducible representation Γ_7, obtained by following

projection operator technique implemented in the SARAh [Wills (2000)], are presented in Table 7.4.

Table 7.4 Basis vectors of the irreducible representations of the space group $Pm\bar{3}m$ appearing in the magnetic representation at the Wyckoff site 1b for the wave vector k = (1/2,1/2,1/2) [After Singh et al. (2013)].

Ireps	Basis vector	Atom (0.5, 0.5, 0.5)		
		m_x	m_y	m_z
Γ_7	ψ_1	0	0	1
	ψ_2	1	0	0
	ψ_3	0	1	0

The irreducible representation Γ_7 is three dimensional and enters once into the representation Γ. This representation therefore corresponds to three basis vector magnetic structure. Fig. 7.6(a) shows the results of Rietveld refinements for x = 0.50 using $Pm\bar{3}m$ space group and magnetic structure corresponding to the Γ_7 representation. It can be clearly seen from the figure. 7.6(a) that the fit between the observed and calculated profiles is good only for the magnetic structure. However, the fit between the observed and calculated profiles for the nuclear peaks is not very good for a few reflections as can be seen from the insets of Fig. 7.6(a).

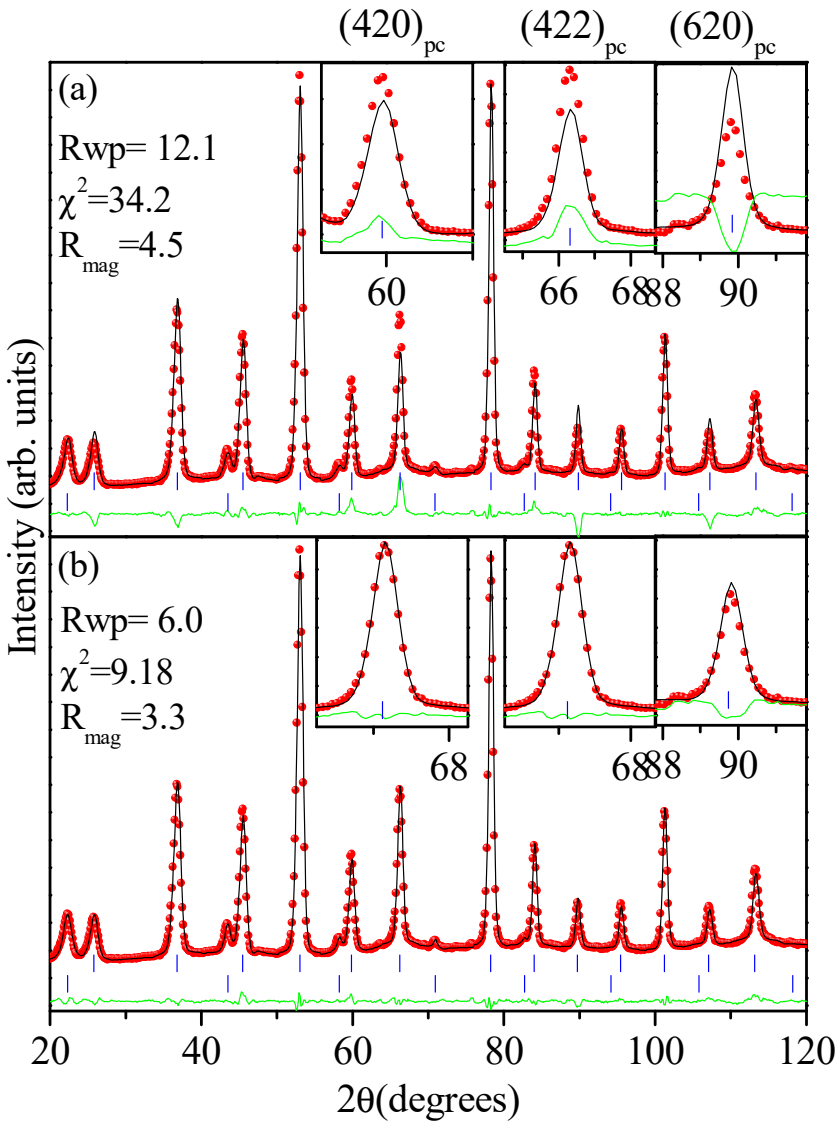

Fig. 7.6 Observed (dots), calculated (solid line), and difference (bottom line) patterns obtained from Rietveld analysis of neutron powder diffraction data of BF-0.50PFN at room temperature using the propagation vector k=(0.5,0.5,0.5) corresponding to the irreducible representation Γ (a) for average cubic structure and (b) disordered Bi^{3+}/Pb^{2+} and O^{2-} atoms along <uuv> and <yy0> directions, respectively, in the average cubic structure with the $Pm\bar{3}m$ space group. The vertical tick marks correspond to the position of all allowed Bragg reflections for the nuclear (top) and magnetic (bottom) reflections.

For nuclear structure refinement <uuv> and <yy0> local disorder models was used for the A-site and O-site ions respectively, as discussed in detail in chapter IV. After considering the local disorder model for the A-site and O-site ions, it was confirmed that Bi^{3+}/Pb^{2+} ions are displaced along <uuv> from their ideal cubic position (0,0,0) by ~ 0.50Å. Oxygen (O^{2-}), on the other hand goes off-center along <110> direction i.e. along the cubic face diagonal by ~ 0.18Å. The values of local displacements for the Bi^{3+}/Pb^{2+} and O^{2-} ions obtained by neutron powder diffraction data is slightly larger than that for the Bi^{3+}/Pb^{2+} ions in comparison to the values obtained by synchrotron x-ray powder diffraction data. For O^{2-} ion, the local displacement value is a little less than that for x-rays. Since the O^{2-} positions are more accurately determined by neutron diffraction, we believe that lower value of local displacement for O^{2-} as compared to that obtained by synchrotron XRD data may be more reliable. The correct O^{2-} local displacement resets the value of local displacement for the Bi^{3+}/Pb^{2+} also. The cubic structure with local displacement of Bi^{3+}/Pb^{2+} and O^{2-} ions gives the lower agreement factors (R_{wp} = 6.0, R_{mag} = 3.30 and χ^2 = 9.18) as compared to that without such displacements (R_{wp} = 12.1, R_{mag} = 4.50 and χ^2 = 34.2) leading to the improvement in the fit between observed and calculated profiles of the nuclear structure shown in Fig. 7.6(b) (see insets also). The refined ordered magnetic moment per Fe^{3+} ion is found to be ~ 3.0 (2) μ_B which is less than the values reported for pure BF in the range of ~ 3.7 to 4.0 μ_B because of the 25% dilution of Fe^{3+} lattice at the 1(b) sites of the cubic perovskite due to Nb^{5+} substitution. The magnetic structure is schematically shown in Fig. 7.7.The results of the Rietveld analysis of neutron diffraction data of BF-xPFN for x = 0.50 are given in Table 7.3.

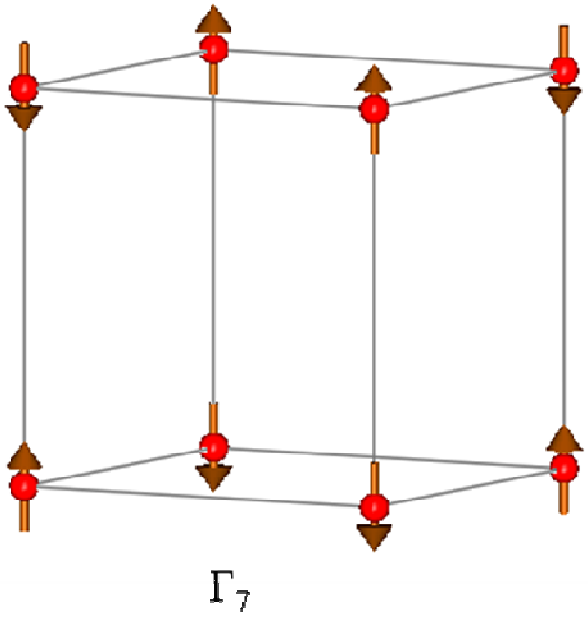

Fig. 7.7 The magnetic structure of BF-0.5PFN corresponding to the irreducible representation Γ_7.

7.4.5 Magnetic structure of the cubic like phase for 0.80 ≤ x < 0.90

The x = 0.80 composition has been considered as the representative composition for Rietveld analysis of the neutron diffraction data in the composition range 0.80≤x<0.90. The room temperature neutron diffraction pattern contains both magnetic and nuclear reflections as shown in Fig. 7.3. Therefore, two phase refinement was carried out to account for the nuclear and magnetic reflections. Since, it has been already shown in chapter IV that the room temperature nuclear structure of the BF-xPFN in the composition range 0.80 ≤ x ≤ 0.90 is cubic ($Pm\bar{3}m$ space group) with local disorder of Bi^{3+}/Pb^{2+} and O^{2-} along <111> and <110> direction respectively, cubic structure with $Pm\bar{3}m$ space group

with and without local disorder model was used for the nuclear structure while the magnetic reflections were account for by using additional phase with a propagation vector k = (0.5,0.5,0.5) referred to the space group $Pm\bar{3}m$. As discussed in the previous section, a G-type of magnetic structure corresponding to the irreducible representation Γ_7 of cubic ($Pm\bar{3}m$) phase is possible. The Fig. 7.8(a) shows the fit between the observed and calculated profiles using $Pm\bar{3}m$ space group and magnetic structure corresponding to the Γ_7 irreducible representation without any local disorder. The fit between the observed and calculated profiles for the magnetic reflections is quite good but the mismatch between the observed and calculated profiles for some of the nuclear reflections is observed as can be seen from the inset of Fig. 7.8(a).

To account for all the nuclear reflections properly, we considered the local displacement model the A-site and O-site ions which improved the fit between the observed and calculated profiles as can be seen from Fig. 7.8 (b) and the inset. The cubic structure with local displacement of Bi^{3+}/Pb^{2+} and O^{2-} ions give the lower agreement factors (R_{wp} = 5.7, R_{mag} = 3.40 and χ^2 = 1.66) as compared to without such displacements (R_{wp} = 5.8, R_{mag} = 3.78 and χ^2 = 3.50) leading to the improvement in the fit between observed and calculated profiles. The refined ordered magnetic moment per Fe atom is found to be ~ 1.5(4) μ_B. The results of the Rietveld analysis of neutron diffraction data of BF-xPFN for x = 0.80 are given in Table 7.3 along with those for x = 0.20 and 0.50.

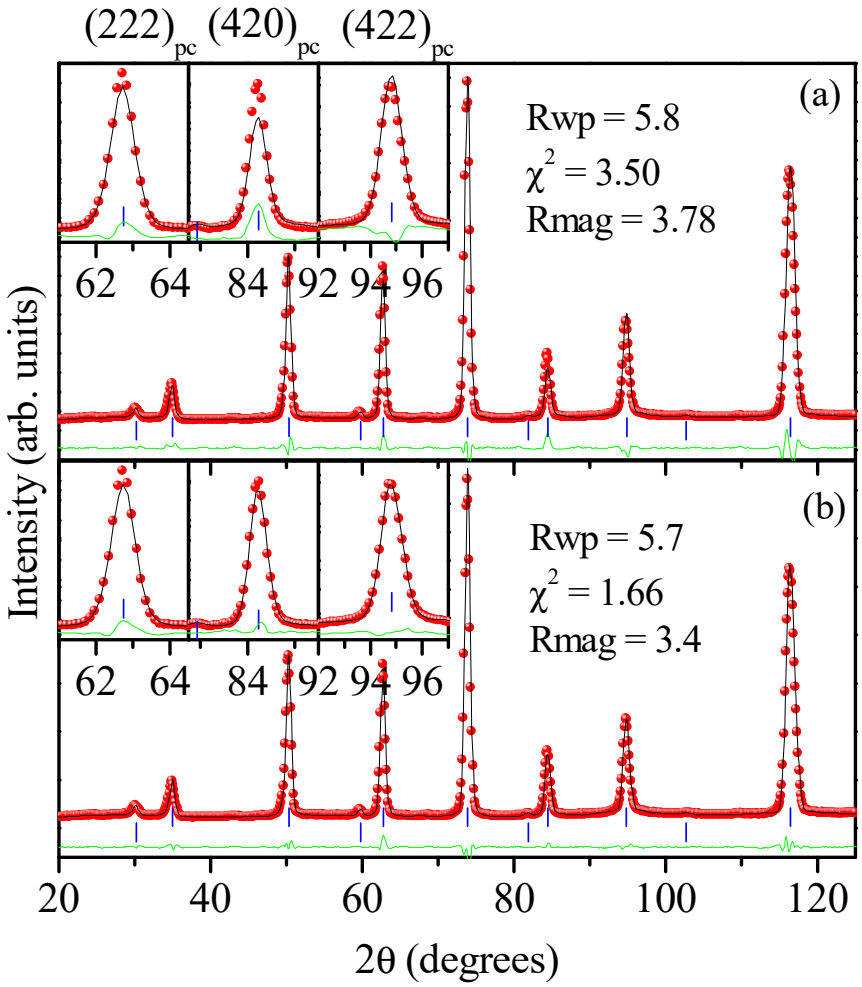

Fig. 7.8 Observed (dots), calculated (solid line), and difference (bottom line) patterns obtained from Rietveld analysis of neutron powder diffraction data of BF-0.80PFN at room temperature using the propagation vector k=(0.5,0.5,0.5) corresponding to the irreducible representation Γ (a) for average cubic structure and (b) disordered Bi^{3+}/Pb^{2+} and O^{2-} atoms along <uuu> and <yy0> directions, respectively, in the average cubic structure with the $Pm\bar{3}m$ space group. The vertical tick marks correspond to the position of all allowed Bragg reflections for the nuclear (top) and magnetic (bottom) reflections.

7.4.6 Rietveld refinement of the nuclear structure of BF-0.9PFN at room temperature

The room temperature neutron powder diffraction pattern of BF-0.9PFN contains only nuclear reflections. No magnetic reflection(s) is observed around the 2θ angle at which the strongest magnetic peak is expected. It has been shown in chapter IV that the average nuclear structure of BF-0.9PFN is cubic with local disorder of Bi^{3+}/Pb^{2+} ions along <111> directions. Therefore, we used $Pm\bar{3}m$ space group based structural models with and without the local disorder of Bi^{3+}/Pb^{2+} ions along <111> directions for the Rietveld refinement of the BF-0.9PFN composition. Figs. 7.9(a) and 7.9(b) depict the Rietveld refinement fit between the observed and calculated profiles for the $Pm\bar{3}m$ space group without and with local disorder, respectively along with the agreement factors. The fit for the local disorder model is better in comparison to the order model as can be seen from inset of Figs. 7.9(a) and 7.9(b). However, only A-site disorder is found for the BF-0.9PFN composition which is consistent with our synchrotron x-ray diffraction study. The local disorder for the O^{2-} ion was found to be absent for this composition. It is worth mentioning that antiferromagnetic ordering exists in the cubic phase of the BF-xPFN for $0.40 \leq x < 0.90$ at room temperature. For the composition $x \geq 0.90$, BF-xPFN shows ferromagnetic like M-H loop at room temperature. The results of the Rietveld analysis of neutron diffraction data for x = 0.90 is given in Table 7.3 along with those for x = 0.20, 0.50, 0.80 and 0.90.

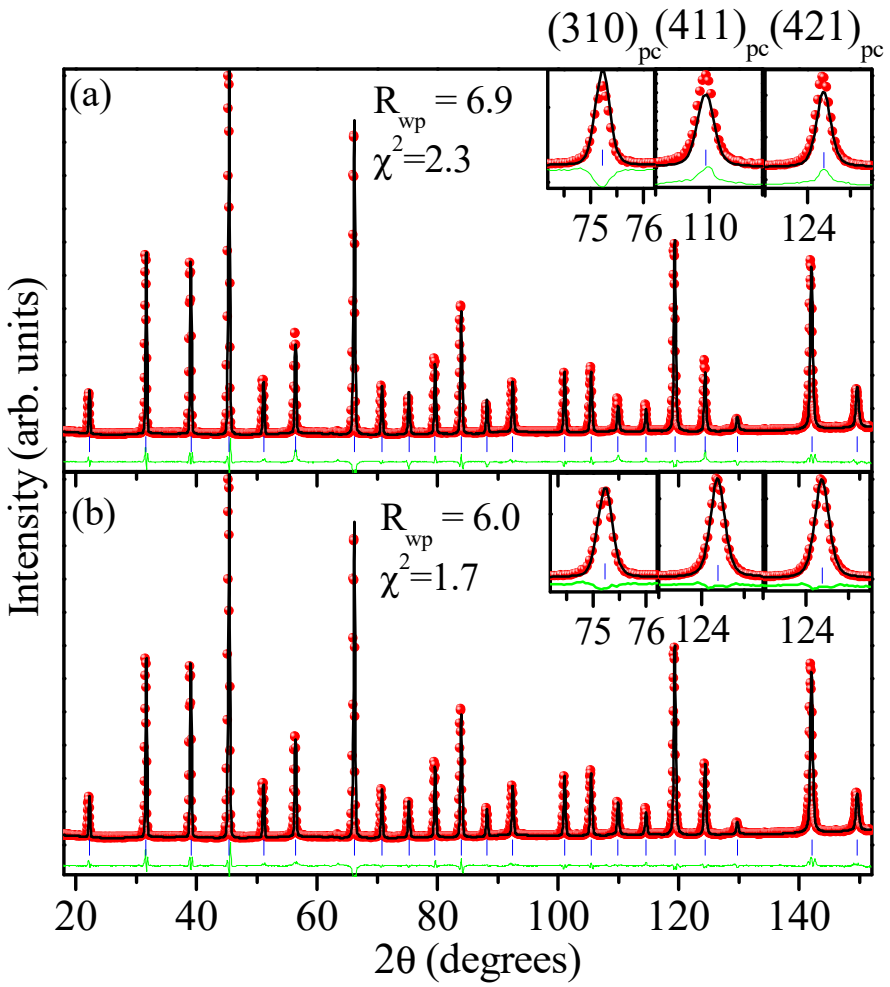

Fig. 7.9 Observed (dots), calculated (solid line), and difference (bottom line) patterns obtained from Rietveld analysis of neutron powder diffraction data of BF-0.90PFN at room temperature using $Pm\bar{3}m$ space group (a) order model (b) disorder model with off-center displacement of Bi^{3+}/Pb^{2+} along <111> directions. The vertical tick marks correspond to the position of all allowed Bragg reflections for the nuclear (top) and magnetic (bottom) reflections.

7.4.7 Variation of magnetic moment of Fe in BF-xPFN as a function of x

Rietveld analysis of the neutron diffraction data in previous section suggests that the room temperature magnetic structure of BF-xPFN is G-type

antiferromagnet in the composition range $0.10 \leq x < 0.90$. Fig. 7.10 depicts the variation of the ordered magnetic moment of Fe sublattice as obtained by Rietveld analysis of the neutron diffraction data at room temperature with increasing concentration of $Pb(Fe_{0.5}Nb_{0.5})O_3$. The magnetic moment of the Fe^{3+} sublattice in BF-xPFN gradually decreases with increasing concentration of $Pb(Fe_{0.5}Nb_{0.5})O_3$ and become zero around $x \sim 0.87$. This reveals that for $x \geq 0.87$ BF-xPFN is not antiferromagnetic at room temperature. The ordered magnetic moment of a magnetic ion in a compound can decrease either by increasing the temperature or by substituting the magnetic ion with the non-magnetic ion. In BF-xPFN solid solution, we are substituting the non-magnetic Nb^{5+} ion at the magnetic Fe^{3+} ion site (B-site in ABO_3 perovskite structure). The $Pb(Fe_{0.5}Nb_{0.5})O_3$ consists of 50% magnetic Fe^{3+} ion and 50% non-magnetic Nb^{5+} ion at their B-site of the perovskite structure.

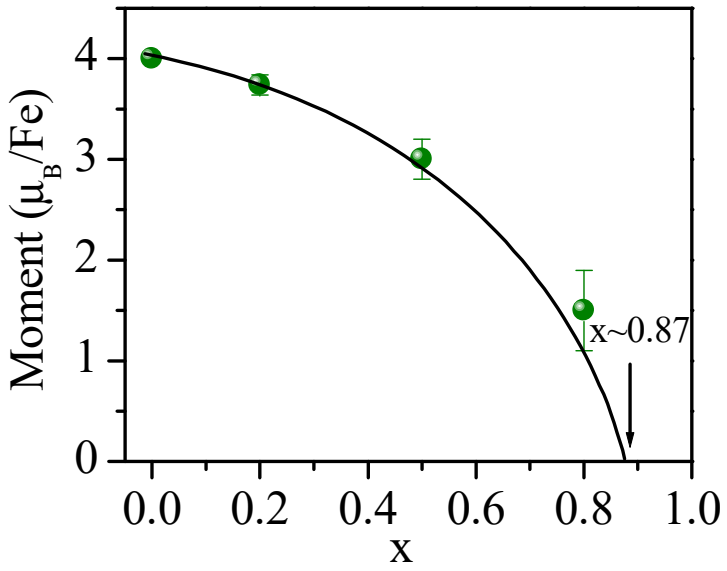

Fig. 7.10 Variation of ordered magnetic moment per Fe^{3+} ion as a function of x in BF-xPFN solid solution.

Increasing the concentration of $Pb(Fe_{0.5}Nb_{0.5})O_3$ in BF-xPFN implies increase in the concentration of non-magnetic Nb^{5+} ion at the B-site of the perovskite structure which dilutes the concentration of magnetic ion Fe^{3+}. The dilution of the concentration of magnetic Fe^{3+} ion weakens the antiferromagnetic superexchange interaction leading to the disappearance of the ordered magnetic structure for $x \geq 0.87$ composition. Before we close, we want to compare our results with the BF-xBT solid solutions because both solid solutions have nearly identical crystal symmetry in whole magnetic phase region. In BF-xBT solid solutions the magnetic ordering disappears at room temperature by substituting ~55% non-magnetic Ti^{4+} ion at the B-site [Singh Ph.D. thesis (2012)] while in the case of BF-xPFN only ~ 43.5% non-magnetic Nb^{5+} ion is sufficient to break the magnetic ordering at room temperature.

7.4.8 Temperature dependent magnetization (M-T) measurements

The magnetic transition temperature and the nature of magnetic ordering can be investigated by magnetization vs. temperature (M-T) measurements. The temperature dependent magnetization measurements were carried out in the composition range $0.10 \leq x \leq 0.90$. Fig. 7.11 depicts the variation of magnetization (M) with temperature for different compositions of BF-xPFN. The magnetization (M) in the composition range $0.10 \leq x < 0.40$ initially increases with increasing temperature and achieves a maximum value at a certain temperature and then decreases sharply with increasing temperature.

This is typical nature of the AFM to PM transition reported for the antiferromagnets [Cullity (1972)]. However, the nature of the M (T) plots slightly changed in the composition range $0.50 < x \leq 0.60$. For these compositions, the magnetization continuously decreases as the temperature goes on increasing with a peak/hump at the Néel temperature. This type of M (T) plot is observed due to weak ferromagnetic behaviour which is also reported for PFN [Yang et al. (2004)]. The BF-xPFN in the composition range $0.6 < x \leq 0.80$ does not shows any hump in their M (T) plots, which may indicate absence of antiferromagnetic ordering in the above composition range. However, the neutron powder diffraction patterns for $x = 0.80$ clearly shows the presence of antiferromagnetic peaks at room temperature. This suggests that the anomaly at Néel temperature for $x = 0.7$ and 0.8 is too weak to be observed in the rising M (T) plot with decreasing temperature. Since no AFM peak(s) is observed in the neutron diffraction pattern of $x = 0.90$ composition, this composition can be either paramagnetic or ferromagnetic at room temperature. However, we do observe a relatively more open M-H loop for this composition as well. Further, the M-T behavior above 400 K shows step characteristics of a ferromagnetic transition. We believe that the magnetic behavior of BF-xPFN is dominated by BF upto $x \leq 0.80$ and by PFN for $x > 0.80$. The Néel temperature (T_N) decreases with increased doping of PFN or by increasing the content of the non-magnetic (Nb^{5+}) ion at the B-site of the perovskite lattice as can be seen from Fig. 7.12. The T_N obtained by the M (T) curves are ~ 600, 566, 539, 500, 450 and 409 K for $x = 0.10$, 0.20, 0.30, 0.40,

0.50 and 0.60 respectively. The critical composition x_C = 0.87 at which antiferromagnetic transition does not occur above 300 K coincides with the critical composition at which the intensity of the magnetic peak disappears.

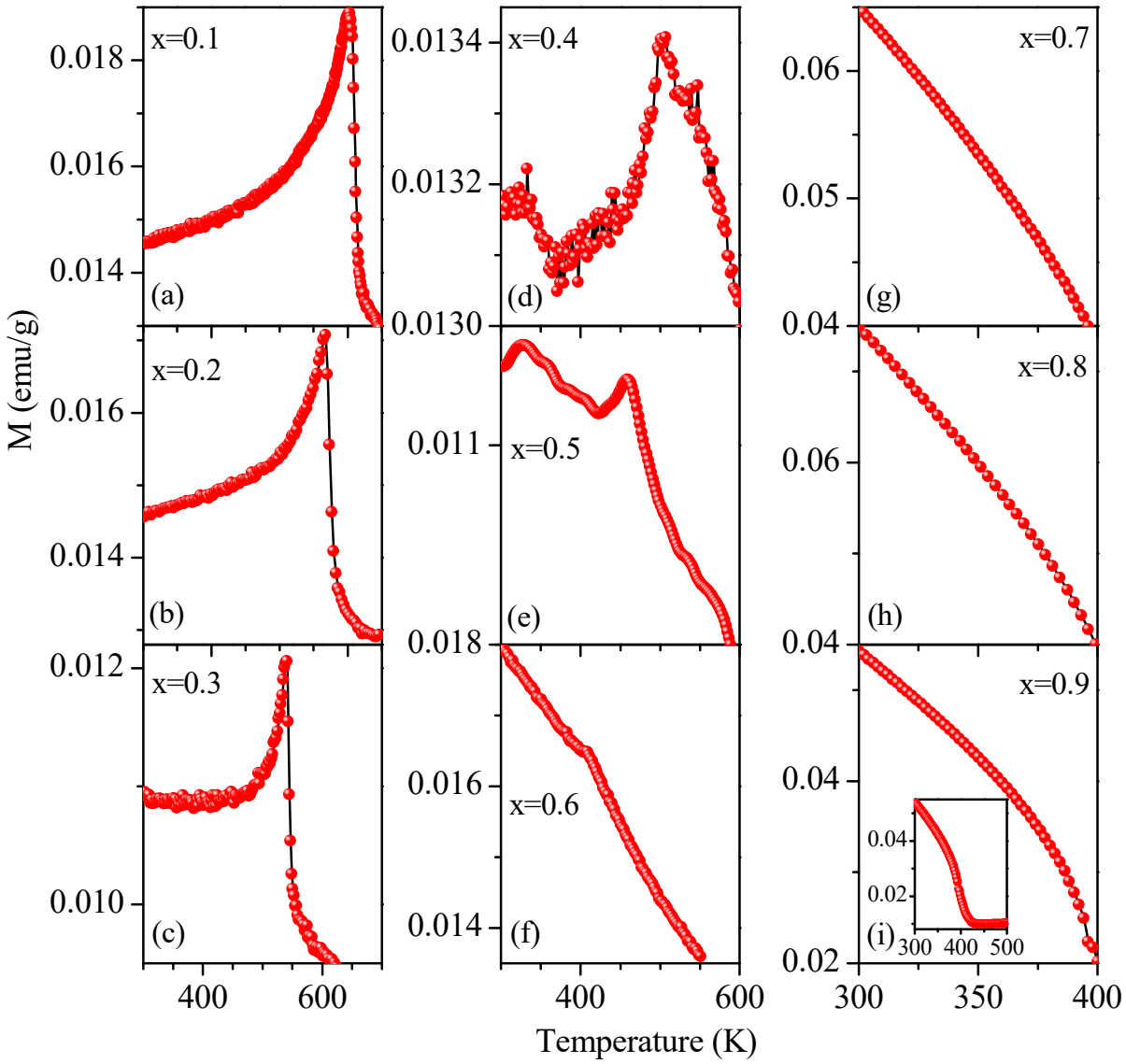

Fig. 7.11 Temperature dependence of dc magnetization (M) measured at 2 kOe applied magnetic field for x = 0.10, 0.20, 0.30, 0.40, 0.50, 0.60, 0.70, 0.80 and 0.90 compositions. Inset in (i) is M (T) curve in full temperature range.

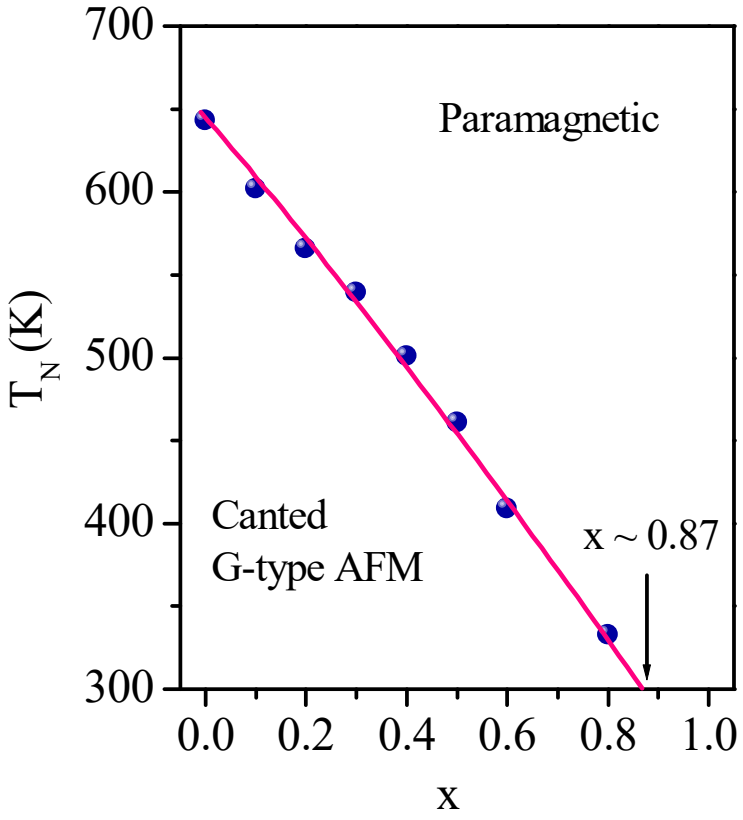

Fig. 7.12 Variation of Néel temperature (T_N) of BF-xPFN as a function of x.

In order to determine the magnetic transition temperature (T_N) of BF-0.8PFN, we have collected the temperature dependent neutron powder diffraction data in the temperature range 2 to 300 K. Fig. 7.13 depicts the neutron diffraction pattern of BF-0.8PFN in the limited 2θ range 28 to 38° at some selected temperatures for clear visibility. It can be clearly seen from the figure that the intensity of the magnetic peak (marked with asterisks (*)) due to the antiferromagnetic ordering decreases with increasing temperature and still persists at the room temperature.

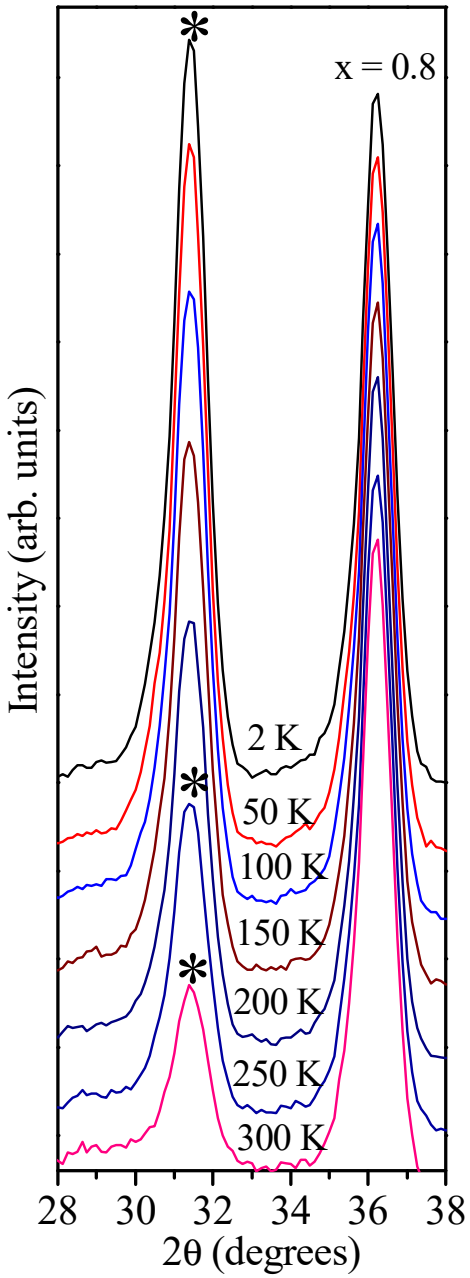

Fig. 7.13 Evolution of the neutron powder diffraction patterns of BF-0.8PFN in the 2θ range 28-38° collected at different temperatures. The asterisks indicate the $(1/21/21/2)_{pc}$ antiferromagnetic peaks.

Fig. 7.14 depicts the temperature dependence of the integrated intensity of the $(1/21/21/2)_{pc}$ antiferromagnetic reflection as a function of temperature. Since

the integrated intensity is directly proportional to square of the order parameter, the integrated intensity plot is fitted by the power law equation $I = I_0(1-T/T_N)^{2\beta}$, where β is the critical exponent. The least square fits are shown by solid line in Fig. 7.14 and it gives the critical exponent $\beta \approx 0.32(1)$ and Néel temperature $T_N \approx 332(1)$ K. Since the M-T measurements were carried out from 300 K onwards, the expected anomaly at $T_N \approx 332$ K could not be observed possibly due to thermal inertia of the high temperature attachment. Measurements starting from well below 300 K could have captured the small anomaly at $T_N \sim 332$ K for x = 0.80.

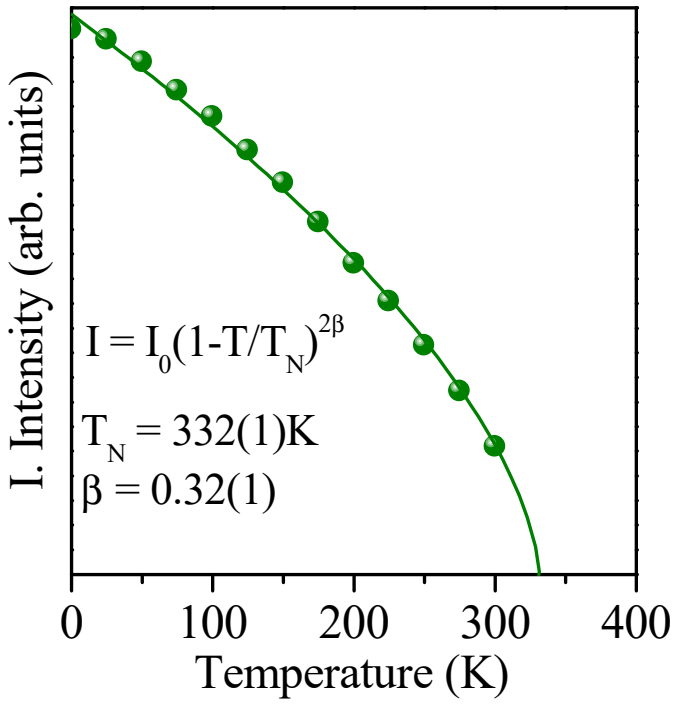

Fig. 7.14 Temperature dependence of the integrated intensity (dots) of the $(1/21/21/2)_{pc}$ antiferromagnetic peak of BF-0.8PFN. Solid line is the fitted curve by using power law equation $I = I_0 (1-T/T_N)^{2\beta}$. Fitted parameters are given in the figure.

7.4.9 Correlation between weak ferromagnetism and crystal structure parameters

The canting of the magnetic sublattices is caused by an antisymmetric spin coupling called as D-M (Dzyaloshinskii and Moriya) interaction, which is due to the combined action of super exchange interaction and spin orbit coupling. The spin Hamiltonian can be expressed [Hill et al. (2008)] as follows: $H = \sum_{ij} \{J_{ij}(S_i \cdot S_j) + D_{ij}.[S_i \times S_j]\}$, where each nearest- neighbour pair ij appears only once in the summation. The first term includes the Heisenberg super exchange interaction and second term due to the D-M interaction [Dzyaloshinskii (1964), Moriya (1960)]. J_{ij} is the super exchange interaction parameter between the nearest neighbour spins, i and j and S are the spin vectors. D_{ij} is the Dzyaloshinskii vector proportional to the spin-orbit coupling constant λ and perpendicular distance of the oxygen (O^{2-}) ion in the Fe^{3+}–O^{2-}– Fe^{3+} chain. If, we neglect the spin orbit coupling term, then Hamiltonian depends only on the super exchange interaction. Super exchange interaction energy is minimum only when the bond angle of Fe^{3+}–O^{2-}–Fe^{3+} is 180° which favours the G-type collinear antiferromagnetic spin ordering. In pure $BiFeO_3$, Fe^{3+}–O^{2-}– Fe^{3+} bond angle is reported to be ~155.3° which is directly linked with oxygen octahedral rotation along [111] direction [Palewicz et al. (2007)]. The deviation of Fe^{3+}–O^{2-}– Fe^{3+} bond angle from 180° in $BiFeO_3$ facilitates the D-M interaction and allows the spins to cant away from their collinear configuration. This leads to weak ferromagnetism [Eibschutz et al. (1967)]. However, the presence of the spatially spin modulated structure (SSMS) (λ ~ 620 Å) in $BiFeO_3$ [Sosnowaska et al.

(1982), Roginskaya et al. (1966)] results in a periodic variation of the canting angle between the Fe sublattices, so that the weak ferromagnetic magnetization averages over the cycloid period is zero. In contrast to $BiFeO_3$, BF-xPFN solid solution exhibits weak ferromagnetic loops. The origin of the weak ferromagnetic loops in the BF-xPFN solid solution is evidently due to the presence of the small spin canting. The spin canting between the two adjacent Fe magnetic moments is facilitated by D-M interaction. In order to explain the occurrences of weak ferromagnetic loops in the BF-xPFN solid solution we have calculated from Rietveld refined position coordinates the composition dependent octahedral rotation angle, $Fe^{3+}–O^{2-}– Fe^{3+}$ bond angle and bond length which are shown in Fig. 7.15. The octahedral tilt angle decreases with increasing x while the $Fe^{3+}–O^{2-} – Fe^{3+}$ angle increases with increasing x in the composition range $0.10 \leq x < 0.40$. The deviation from 180° angle of the $Fe^{3+}–O^{2-}–Fe^{3+}$ linear chain decreases the perpendicular distance of the O^{2-} ion from the linear $Fe^{3+}–O^{2-}– Fe^{3+}$ chain position and hence decreases the D-M interaction because $D_{ij}\alpha\ \lambda(X*r_{12})$ [Cheong et al. (2007)] where, "X" is the perpendicular distance of the O^{2-} ion in the $Fe^{3+}–O^{2-}– Fe^{3+}$ non-linear chain. This indicates that D-M interaction and hence spin canting decreases with x in the composition range $0.10 \leq x \leq 0.40$. This implies that the remanent magnetization (M_r) should decrease with increasing x in the composition range $0.10 \leq x < 0.40$.

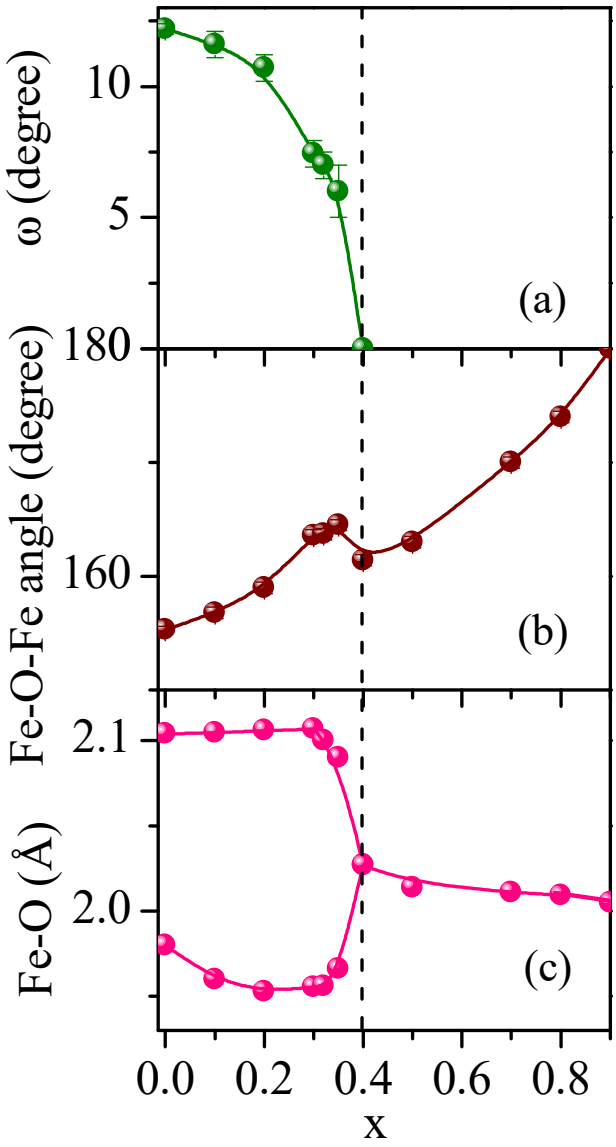

Fig. 7.15 Variation of (a) tilt angle (b) Fe-O-Fe bond angle (c) Fe-O bond lengths as a function of x in BF-xPFN solid solution.

However, our magnetization results indicate that M_r initially increases with x and achieves a maximum value at x ≈ 0.10, and after that it decreases linearly with x. The initial trend of the M_r versus x plot could only be explained in terms of the gradual melting of the spiral spin structure of $BiFeO_3$ with increased doping of $Pb(Fe_{0.5}Nb_{0.5})O_3$ and hence the release of the locked-in magnetization due to the

spiral ordering. However, we do not have any experimental data for x< 0.10 to capture the rising trend of M_r shown in Fig.7.2. It is also possible that there is no peak in M_r at x = 0.10, the M_r just appears above a critical composition required to melt the spin spiral. The M_r at x = 0.10 composition is attributed to the complete suppression of the spiral spin structure of the $BiFeO_3$. However, the locked-in or latent magnetization is very small $M_r \sim 0.0038$ emu/g in comparison to the $M_r \sim 0.15$ to 0.30 emu/g reported due to the suppression of the spiral spin structure of $BiFeO_3$ by solid solution formation at room temperature [Popov et al. (1993), Catalan et al. (2009), Wang et al. (2005)]. The observed very small value of M_r for BF-xPFN system indicates that the canting angle becomes very small in the presence of Nb^{5+} nonmagnetic ion in the Fe^{3+} lattice.

The octahedral tilt angle gradually decreases with increasing concentration of $Pb(Fe_{0.5}Nb_{0.5})O_3$ and completely disappears at the first morphotropic phase boundary (MPB) around x = 0.40. The first MPB is due to the rhombohedral (R3c) to cubic ($Pm\bar{3}m$) phase transition discussed in chapters III and IV. For the ideal cubic structure with $Pm\bar{3}m$ space group, the Fe^{3+}–O^{2-}– Fe^{3+} angle should be 180° and should therefore forbid the possibility of the canted spin structure. This would contradict the observed weak magnetic behaviour for $x \geq 0.40$ compositions. However, the local structure refinement in the composition range $0.40 \leq x \leq 0.87$ reveals that O^{2-} ion is locally displaced along the <110> direction i.e. along the face diagonal of the cubic structure. The local displacement of the O^{2-} ion along the <110> direction in the cubic phase of BF-xPFN solid solution demonstrates the existence of local octahedral tilt in the composition range $0.40 \leq x \leq 0.87$

[Singh et al. (2014)]. The local octahedral tilt indicates the oxygen ion (O^{2-}) is displaced in the perpendicular direction of the Fe^{3+}–O^{2-}– Fe^{3+} linear chain and reduces the Fe^{3+}–O^{2-}– Fe^{3+} angle from 180°. After getting a dip in the Fe^{3+}–O^{2-}–Fe^{3+} angle at the first MPB (x = 0.40) it linearly increases with x and has values less than 180° in the composition range $0.40 \leq x \leq 0.87$ as can be seen from Fig. 7.15(b). This observation suggests that canted spin structure is allowed by D-M interaction even in the cubic phase of the BF-xPFN solid solution due to local O^{2-} disorder. The weak magnetic moment of BF-xPFN solid solutions not only depends on the structural parameters but also depends on the concentration of the magnetic Fe^{3+} ion in the B-sublattice of the cubic perovskite. The concentration of the Fe^{3+} ion decreases with increasing concentration of non-magnetic Nb^{5+} ion at the B-site of the cubic perovskite with increasing x. Therefore, for $x > 0.60$ dilution effect dominates over the structural parameters and hence results in very small value of the M_r. This implies that M_r should decrease with increasing the concentration of non-magnetic Nb^{5+} ion at Fe^{3+}sublattice. But M_r increases with x for $x \geq 0.6$ with an anomaly at x~0.90. We argue that this is due to the dominating effect of PFN. PFN is G-type antiferromagnet below room temperature with T_N ~143 K. It shows weak unsaturated ferromagnetic loops with remanent magnetization (M_r) in the range of 0.06-0.10 emu/g in the temperature range 2-5 K [Blinc et al. (2007), Kumar et al. (2007)]. It has been reported that PFN also shows M_r of the order of ~0.05 emu/g above its antiferromagnetic to paramagnetic transition temperature (T_N) [Blinc et al. (2007)]. In the BF-xPFN solid solution, we expect the M_r above $x \geq 0.87$ composition i.e. in the paramagnetic region is

purely due to the PFN effect while in the composition range $0.60 \leq x \leq 0.87$partial contributions is due to both the spin canting and the PFN doping effect. Fig. 7.15 (c) also depicts the variation of the Fe-O bond length with x which gives the information about the polar displacement of Fe^{3+} ion rather than tilting of the oxygen octahedral for R3c space group. The short Fe-O and long Fe-O bonds are initially getting separated with increasing x up to the composition x = 0.30 after that they approached each other and got equal values at the first MPB x = 0.40. For x > 0.40, the Fe-O bond decreases with increasing x. However, the local displacement of Bi^{3+}/Pb^{2+} ions in the average cubic lattice leads to ferroelectric polarization in the so-called 'cubic' phase.

7.5 Summary and conclusion

The findings of this chapter can be summarized as follows:

(i) Weak ferromagnetism is observed in BF-xPFN solid solutions for $0.1 \leq x < 0.96$ compositions. The maximum value of the remanent magnetization $M_r \sim 0.0038$ emu/g is observed for x = 0.10 in the composition range $0 < x < 0.60$.

(ii) The observation of the weak ferromagnetism in BF-xPFN solid solution is attributed to suppression of spatially modulated spiral spin structure of $BiFeO_3$ to a homogenous spin structure.

(iii) We have investigated the room temperature magnetic structure of BF-xPFN solid solutions by analyzing the neutron powder diffraction data using group theoretical representation theory. The G-type antiferromagnetic spin structure is observed both in the rhombohedral (with R3c space group) and the average cubic ($Pm\bar{3}m$ space group) phases for their magnetic structures.

(iv) The composition variation of ordered magnetic moment of Fe^{3+} demonstrates that BF-xPFN is paramagnetic for $x \geq 0.87$.

(v) The magnetic transition temperature (T_N) decreases linearly with increased doping of $Pb(Fe_{0.5}Nb_{0.5})O_3$.

(vi) The weak remanent magnetization observed in the BF-xPFN solid solution is attributed to canting of the spins. The canting of spins in the non-collinear Fe^{3+}-O^{2-} − Fe^{3+} chain occurs due to D-M interaction. The non-collinear Fe^{3+}−O^{2-}−Fe^{3+} chain arises due to the octahedral tilt in the rhombohedral phase while because of local oxygen disorder in the average cubic phase.

(vii) The origin of anomalous M-T behavior with a ferromagnetic like transition well above M-T for $x \geq 0.87$ seems to be due to doping of PFN with BF whereas the weak ferromagnetism for $x < 0.87$ is due to doping of BF with PFN.